Experimental Study on a Low-Power Direct Current Arcjet

Hitoshi Kuninaka,* Masahiro Ishii* and Kyoichi Kuriki†
Institute of Space and Astronautical Science, Tokyo, Japan

An experimental investigation on a low-power dc arcjet with helium propellant was conducted. Objectives were to evaluate the thermal efficiency, to assess the performance of various cathode materials, and to investigate the effects of transpirational cooling from the electrodes. The anode was made of porous tungsten so that the propellant could be supplied through the anode. The cathode materials used in this experiment were porous tungsten, thoriated tungsten, lanthanum hexaboride, and porous tungsten impregnated with barium oxide (BaO/W). Two discharge modes of low and high voltages were found, which corresponded to low and high thermal efficiency, respectively. The BaO/W cathode was the best of all the tested materials, demonstrating a thermal efficiency as high as 64.9%. The transpirational cooling resulted in a great decrease of the thermal efficiency.

Introduction

DIRECT-CURRENT (dc) arcjet engines were developed vigorously in 1960s.[1] In those days, the arcjets of medium power (20-50 kW) had almost reached the stage of final development, exhibiting excellent results in endurance tests.[2,3] However, arcjets operated in this power range may not be required until the era of the evolutionary space station. Therefore, an arcjet operated in the low-power range (1-3 kW) has priority for near-future development.

The problems of the low-power dc arcjets are low thrust efficiency, short lifetime, and unstable operation. The low efficiency results for the following reasons peculiar to the low-power dc arcjets: 1) the frozen flow loss amounts to a great part of input power; 2) because of the low propellant mass flow, heat losses dissipated from the electrodes are only slightly recovered by regenerative cooling, which is more efficient for arcjets in the larger power ranges; and 3) because of the small nozzle throat diameter, the nozzle efficiency becomes lower. For the same reasons, the electrodes are exposed to a severe thermal environment and their lifetime is therefore shorter. The electrode erosion results in unstable operation, as evidenced by high voltage, luminosity fluctuation, and erosion debris in an exhaust.

In an arcjet, a propellant is heated in an arc discharge to a very high temperature and becomes a partially ionized plasma. As it emanates from a nozzle, thermal energy is converted into kinetic energy and recovers some ionization energy through the recombination reactions. The total thrust efficiency is the product of the thermal, nozzle, and frozen flow efficiencies. The nozzle efficiency is determined by the nozzle configuration. The frozen flow efficiency depends strongly on the recombination relaxation rate of a used propellant.[4] Although the latter two problems are still open to investigation, the present study is focused on the improvement of the thermal efficiency. The power deposited in the electrode fall regions does not contribute to the heating of the propellant, but does cause heating of the electrodes. Hence, a decrease in the fall voltage by using a highly electron-emissive material for the electrodes will enhance both thermal efficiency and durability. It is also advantageous if the power deposited into the electrodes is regeneratively recovered. Transpirational cooling is promising. In this scheme, the propellant is supplied from the porous electrodes into the discharge region. A free-burning discharge with anode transpirational cooling was tested in a previous work.[5] Constricted arc discharges have been studied by a numerical analysis.[6]

In the present experiment, a low-power dc arcjet using a helium propellant was studied in order to evaluate the thermal efficiency, to assess the performance of various cathode materials, and to investigate the effects of the transpirational cooling from the electrodes.

Experimental Equipment

Helium is employed as the working gas. Generally, gases of lower molecular weight have higher frozen flow efficiencies. Although hydrogen is used as a propellant in most MHD applications, helium is substituted here because of its experimental safety when the gas lines are imperfectly sealed. In the present experiment, the atmosphere is 99.995% helium.

The electrode configurations are conventional, as shown in Fig. 1 except for the transpirational gas feeding capability. The specifications of the electrodes are summarized in Table 1. Porous tungsten, used for both the anode and the W cathode, is sintered with powder having a 5 μm mean particle diameter and 28% porosity. The mass flow rates from the porous anode are 10 mg/s in the cold condition and 5 mg/s with the arc discharge on and in thermal equilibrium. The same orders of mass flow rates are found in the W cathode. The change in the mass flux distribution on the electrode surfaces due to arc discharge could not be measured.

Figure 2 is a schematic view of the experimental setup. The vacuum chamber of stainless steel is 0.6 m in diameter and 2 m long and is evacuated by rotary and mechanical booster pumps whose pumping speed is 3500 m^3/h. During the experiment, the background pressure is kept below 0.1 Torr in the vacuum chamber. The discharge power is supplied by a constant-current dc power of 100 A and 200 V maximum rating. An open-circuit voltage of 400 V causes breakdown. The discharge current and voltage were measured by series and shunt resistors of 1 mΩ and 5 kΩ, respectively. The propellant supply system has three feed lines: the anode transpirational injection (ATI), the cathode transpirational injection (CTI), and direct injection (DI) between the electrodes. The propellant is supplied by either DI alone or combined with other systems. The mass flow rate (which is 20-90 mg/s) is controlled by adjusting the orifices and reservoir pressure and is measured by pressure gages and flow meters. In order to measure the heat transfer to them, the electrodes are cooled by water. The enthalpy of the working gas in the arc discharge is

Received Jan. 9, 1986; revision received May 9, 1986.

*Presently, Graduate Student, University of Tokyo.
†Professor. Member AIAA.

measured from the pressure in the plenum chamber by means of a pressure rise technique.[7]

Experimental Results

Discharge Characteristics

It took about 30 min for the equipment to establish a thermal equilibrium after the beginning of the arc discharge. All measurements were performed in the equilibrium condition. In course of the study, the gas leak from a brazed point on the anode copper disk prevented the anode transpirational injection of the working gas. The anode melting was insignificant for about 10 h, after which it was replaced with a spare anode. The LaB_6 cathode was likely to break into pieces during operation and the W cathode was affected by severe erosion at its tip. Cathodes made of other materials kept their original shapes over the entire test period.

Two distinctly different discharge modes were found while measuring the discharge characteristics: 1) low mode, which in general corresponds to low discharge voltage and low pressure in the plenum chamber, and 2) high mode, corresponding to high voltage and pressure. All of the results obtained with W, ThW(45), and LaB_6 fell within the low mode. Both modes were found in the cases of ThW(20) or BaO/W. Below 60 A, the discharge was in the high mode; above 70 A, it turned into the low mode. In the case of the low mode, stain and minor debris were found, primarily at the entrance of the constrictor. On the other hand, in the high mode, most of the debris was found at the nozzle. More definite groupings will be given in the next section.

Figure 3 presents the voltage/current characteristics of the arc discharge measured for three mass flow rates, 68.9, 43.1, and 25.8 mg/s. It is shown here that the voltage decreases with increasing current. Also, the voltage increases with increasing mass flow rate. This may imply that a larger amount of propellant requires a larger power to both heat and ionize it. Another explanation is that the higher voltage may be associated with the longer positive column.

The voltage measured for three different anode/cathode gaps (4.2, 2.2, and 0.7 mm) are represented in Fig. 4. The voltage becomes higher as the gap becomes wider in the current range shown. The longer positive column is considered to cause the higher voltage.

The current/voltage characteristics with DI only are compared in Fig. 5 for the different cathode materials. The higher voltages are found for ThW(20), W, BaO/W, ThW(45), and LaB_6 in that order.

The difference in the voltage with and without ATI in the low mode is shown in Fig. 6. The primary gas injection system is DI and the mass flow rate of ATI is 5 mg/s. The voltage is enhanced when ATI is added. In general, an increase in the mass flow rate results in a voltage rise, as seen in Fig. 3. The voltage increase due to the addition of ATI is larger than that obtained with the increase of the DI mass flow rate.

Thermal Characteristics

The thermal efficiency η_a is defined by

$$\eta_a = \dot{m}H/(\dot{m}H_0 + IV) \tag{1}$$

where $\dot{m}$ is the mass flow rate, H the gas enthalpy with discharge, H_0 the gas enthalpy without discharge, and IV the electrical input power. Because of a low ionization rate, the

Table 1 Electrodes

Electrode	Anode	Cathode W	Cathode ThW (45)	Cathode ThW (20)	Cathode LaB_6	Cathode BaO/W
Material	Porous tungsten porosity 28%	Porous tungsten porosity 28%	Thoriated tungsten 2% thoria	Thoriated tungsten 2% thoria	Lanthanum hexaboride	Porous tungsten impregnated with barium oxide
Size	Constrictor diameter 3mm length 7.8mm	Diameter, mm 10	5	5	5	5
	Nozzle area ratio 10	Cone angle, deg 45	45	20	45	45

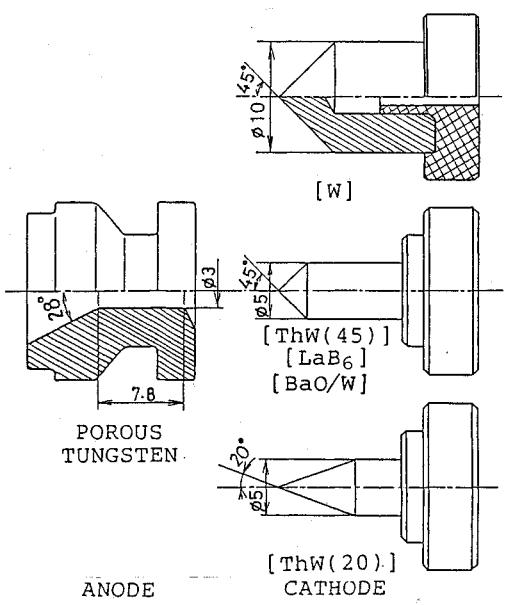

Fig. 1 Configuration of electrodes.

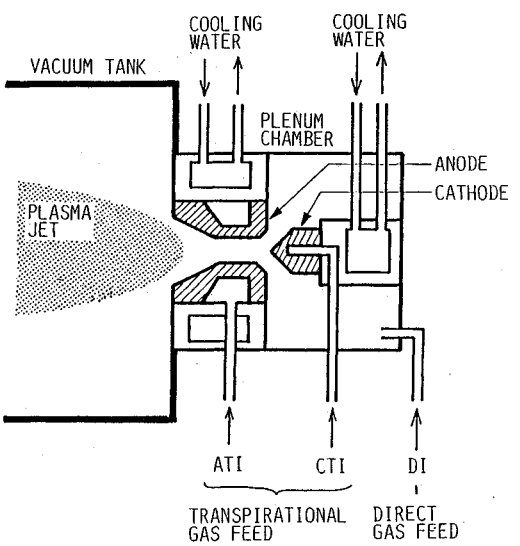

Fig. 2 Test equipment and facility.

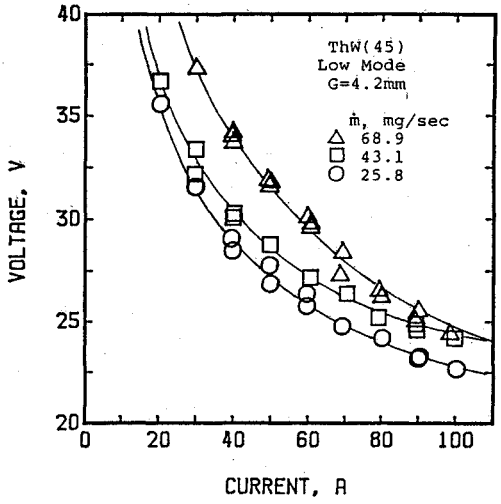

Fig. 3 Voltage-current characteristics for various mass flow rates with DI only.

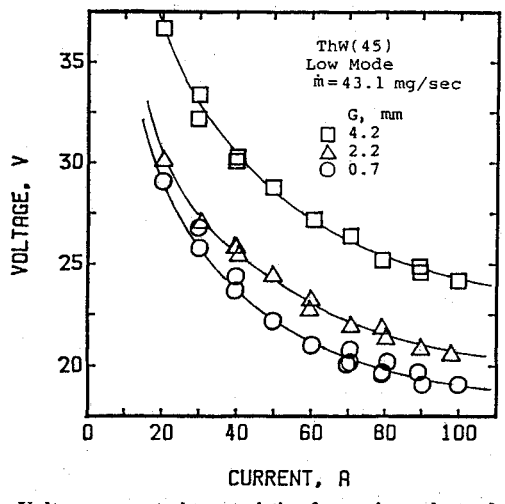

Fig. 4 Voltage-current characteristics for various electrode gaps G with DI only.

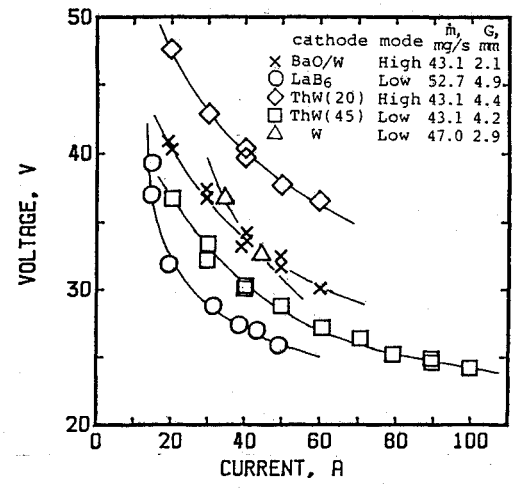

Fig. 5 Voltage-current characteristics for various cathode materials with DI only.

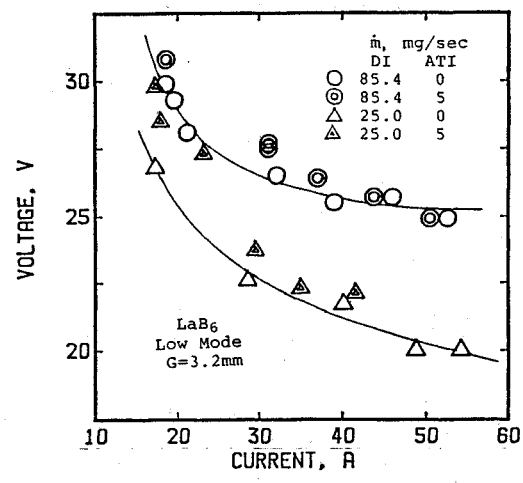

Fig. 6 Voltage-current characteristics with and without ATI.

thermal efficiency can be expressed by the alternative form η_b

$$\eta_b = 1 - P_L/(\dot{m}H_0 + IV) \tag{2}$$

where P_L is the electrodes power loss.

In Fig. 7 the thermal efficiency with DI only is plotted against the discharge current and compared for the different cathode materials. The thermal efficiency in this figure is referred to as η_a. The measured η_a and η_b are found to be in close agreement. The highest value is obtained with the BaO/W cathode and the lowest with the W cathode. It can be seen that the high and low modes of the same ThW cathode correspond to the high and low efficiency, respectively.

Figure 8 shows the effect of the anode transpirational cooling on the thermal efficiency. The results were obtained with and without ATI in the low mode. ATI degrades the thermal efficiency drastically when used at a low mass flow rate. At a high mass flow rate, the thermal efficiency is rather insensitive to ATI. The effect of ATI on the high mode operation could not be confirmed due to the failure of the brazing on the anode piece. From the general behavior, however, ATI for the high mode is expected to be unfavorable.

When CTI was used, the arc discharge became unstable. In the case of a low-power arcjet, i.e., of about 1 kW, the active cooling deprives too much heat from the cathode and reduces the electron emission. Therefore, the cathode transpirational cooling is concluded to be superfluous in the present experiment.

The cathode heat loss is plotted in Fig. 9 against the total power, i.e., the sum of the electrical input power and the enthalpy of the cold gas. The heat loss for the W cathode is as much as 6% of the total power. The losses for other types of cathode fall below this value.

Cathode Erosion

The cathode mass loss was measured after an operation for a certain time period. As a conventional experimental expression, the specific mass loss is defined as the total mass loss divided by the total electric charges passed in the arc discharge. The results are overestimated, since the data are affected by severe erosion due to an unstable condition occurring at the start of the discharge. The results are plotted in Fig. 10 vs the work functions of the cathode materials. The specific mass loss is found to increase with the work function, except for the LaB_6 cathode; this cathode was often found to be broken into pieces, especially in the starting phase of the arc discharge and during the changes in the operational parameters. Pure tungsten at elevated temperatures is subject to rapid oxidation at even trace amounts of O_2. The 99.995% pure helium includes less than 5 ppm oxygen, which amounts to 0.3 μg/s at $\dot{m} = 68.9$ mg/s. The atmospheric oxygen leakage of the vacuum tank amounts to 4×10^{-4} μg/s. Therefore, the former is more effective if oxidation is the responsible mechanism for the cathode mass loss.

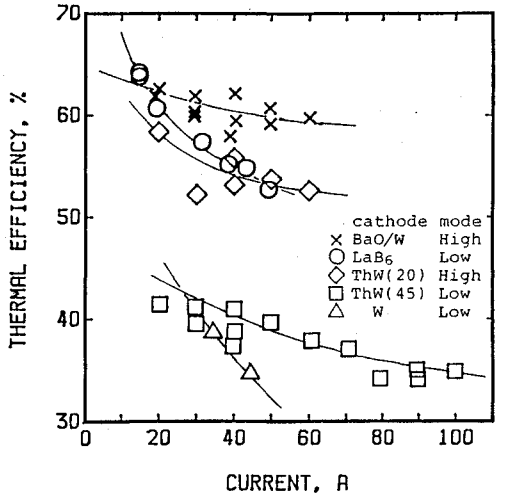

Fig. 7 Thermal efficiency η_a vs current for various cathode materials.

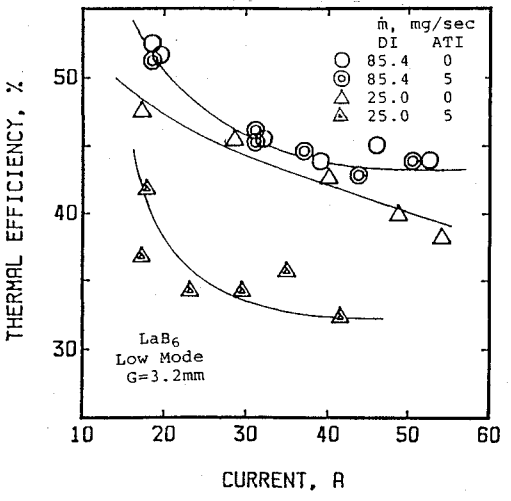

Fig. 8 Thermal efficiency η_a vs current with and without ATI.

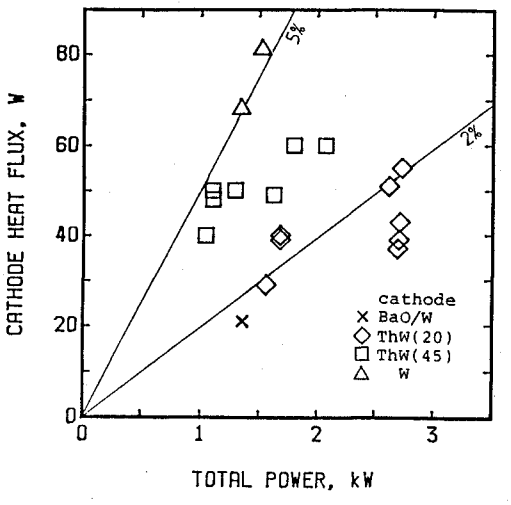

Fig. 9 Cathode heat loss for various cathode materials.

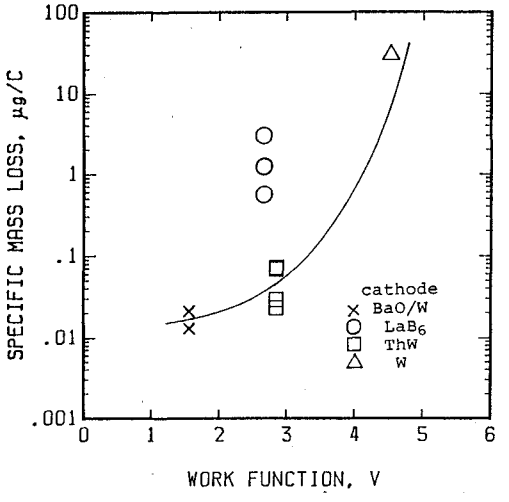

Fig. 10 Specific mass loss vs work function of cathode materials.

Discussion

Discharge Mode

In general, the overall discharge voltage V_0 is expressed by the equation

$$V_0 = V_a + V_c + V_p \tag{3}$$

where V_a is the anode fall voltage, V_c the cathode fall voltage, and V_p the positive column voltage.

For the arc discharge occurring in the nozzle, the electric potential varies along the positive column. When an average electric field in the positive column is expressed as E, Eq. (3) is rewritten into

$$V_0 = V_f + EL \tag{4}$$

where $V_f = V_a + V_c$ and L is the length of the positive column.

The voltage V_f depends on the current and pressure in the arc discharge and the electrode material. However, for currents above 10 A, the pressure dependence for V_f disappears.[8] The anode fall voltage V_a is possibly dependent upon the modes of anode attachment, i.e., the spot or diffuse mode. However, V_a is as large as 5 V, whereas the cathode drop V_c is 10-20 V. Therefore, the total electrode fall voltage V_f is rather insensitive to V_a, even when V_a is affected by the anode attachment. The electric field E is determined by the balance of Joule heating and thermal dissipation. With regard to the arc discharge in the nozzle flow, E is experimentally found to be proportional to the 0.8 power of the pressure.[9] The pressure at each point in the nozzle can be expressed by the plenum chamber pressure P_0 when the flow is assumed to be one-dimensional, stationary, and in thermal equilibrium. Describing the proportional constant as β, E is expressed by

$$E = \beta P_0^{0.8} \tag{5}$$

The length L is the sum of the electrode gap G and an unknown length L_0. Therefore, Eq. (4) is rewritten as

$$V_0 = V_f + \beta P_0^{0.8}(G + L_0) \tag{6}$$

The unknown values V_f, β, and L_0 can be determined from the measured values V_0, P_0, and G at a constant current by the least squares method. V_0 vs $P_0^{0.8}(G+L_0)$ is plotted for different currents in Fig. 11. All points lie on the straight line within a 10% deviation. L_0, β, and V_f are plotted for the various cathode materials vs the current in Figs. 12-14, respectively. In Figs. 12 and 13, two groups are distinctly found. One corresponds to small L_0 and large β and is classified as the low mode. The other is the high mode corresponding to large L_0 and small β. Because L_0 is almost zero in the low mode, the length of a positive column is equal to G. In this case, the arc touches at the upstream end of the constrictor as shown in Fig. 15a. Alternatively, in the high mode, a long positive column is formed as shown in Fig. 15b. The voltage V_f does not depend

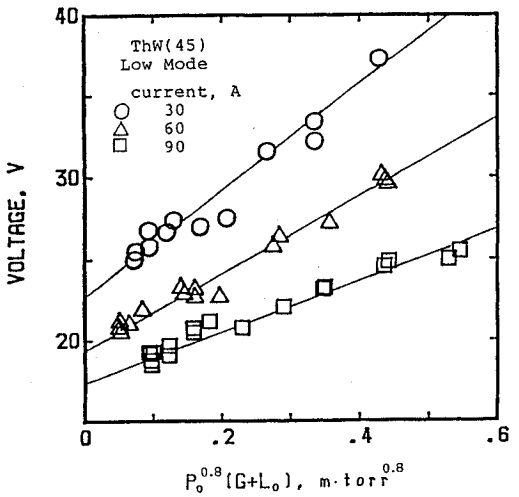

Fig. 11 Linear dependence of discharge voltage on $P_0^{0.8}$ $(G+L_0)$.

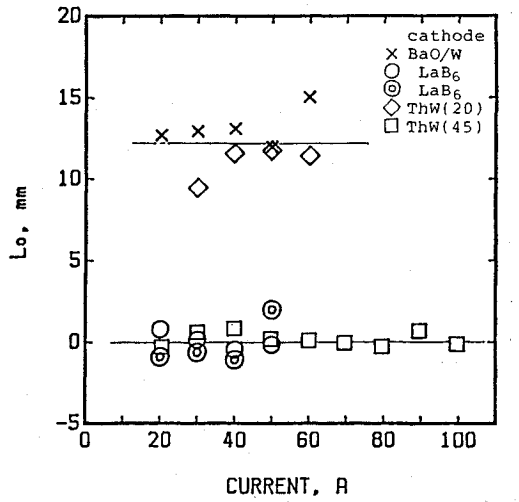

Fig. 12 L_0 vs current characteristics for various cathode materials.

on the discharge mode but, rather, on the cathode material. This is demonstrated in Fig. 14, where the V_f values of the same electrode material agree well with each other, irrespective of low and high modes. In the high mode, because of the longer positive column and higher pressure, the voltage is generally higher than in the low mode. Since the ratio of the positive column voltage V_p to the overall voltage V_0 is large, the high thermal efficiency is obtained in the high mode, as shown in Fig. 7. However, the larger area of the constrictor is damaged by high temperatures.

The discharge mode is strongly dependent on both the material and shape of the cathode. As for the material dependence, the difference between BaO/W and ThW(45) is typical, i.e., the former is classified the high mode and the latter is the low mode. On the other hand, the shape dependence is apparent from the difference between ThW(45) and ThW(20) in Figs. 12 and 13. More detailed discussion will be given in the next section.

Cathode Materials

The cathode material of the lower work function emits more electrons under the same conditions and reduces the power for electrons to overcome the Fermi potential. The lower work function makes the electrode fall voltage lower and the thermal efficiency higher as seen in Figs. 14 and 7, respectively. The work function plays an essential role in cathode erosion.

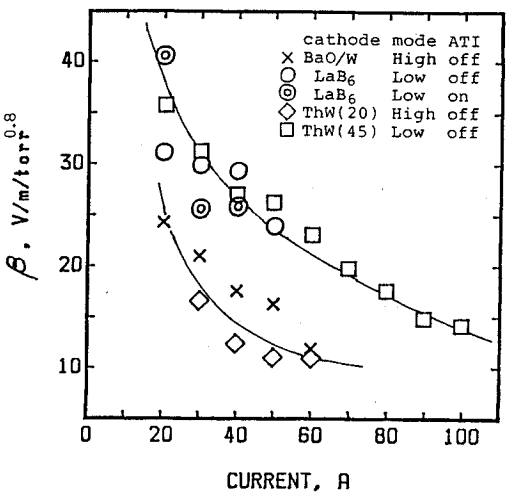

Fig. 13 β vs current characteristics for various cathode materials.

The sputtering by ion bombardment is considered to be responsible for the cathode erosion at small discharge currents. The amount of erosion depends on the ion energy provided by the electrode fall voltage. As shown in Fig. 10, the cathodes of the lower work functions are less affected by such erosion. The threshold energy of the sputtering is dependent upon the electrode material as well as the ion species. Therefore, the decrease of the electrode fall voltage below the threshold extends the electrode life significantly.

The wear of the LaB_6 cathode does not result from the sputtering, but from the thermal shock. The rapid, local heat input mechanically destroys the cathode by local thermal expansion. The second thermal shock coefficient $\sigma_B/\alpha C_e$ is 0.5 for the LaB_6 cathode and 130 for the W cathode, where σ_B is the tensile strength, C_e the elastic coefficient, and α the thermal expansion coefficient. The LaB_6 cathode is found to be very brittle.

From the foregoing discussions, the BaO/W cathode is the best of those tested with respect to thermal efficiency, erosion, and thermal shock. Another item to be taken into account is the endurance for a prolonged mission. The BaO/W cathode is made of a porous tungsten matrix impregnated with barium oxide and calcium aluminates. This impregnated material, which is carried near the surface by capillary action, becomes an efficient electron-emissive material by its chemical reactions. The emission function is lost by its exhaustion or by a choke of the capillary, which occurs with the accumulation of the reaction wastes. Therefore, thermal control of the cathode is required so as not to accelerate its reaction more than necessary.

As mentioned above, the cathode conditions affect the high and low discharge modes. The material dependence specifically means the difference of the work functions. The cathode shape influences the temperature of the cathode tip. A decrease in the work function or a rise in the tip temperature makes the cathode supply more electrons to the arc column. At a given anode throat and constrictor length, the amount of electrons that can be provided from the cathode seems to determine the discharge mode. Although its work function is lower than that of ThW, the discharge for LaB_6 was found to be in the low mode. It may be the reason that the tip shape of LaB_6, which is easily rounded by erosion, prevents its temperature rise.

Transpirational Cooling

The heat losses from the cathodes are found to be less than 6% of the total power, as shown in Fig. 9. The amount of heat is required only to keep the temperature of the cathode high enough to supply electrons. The power recovered by transpira-

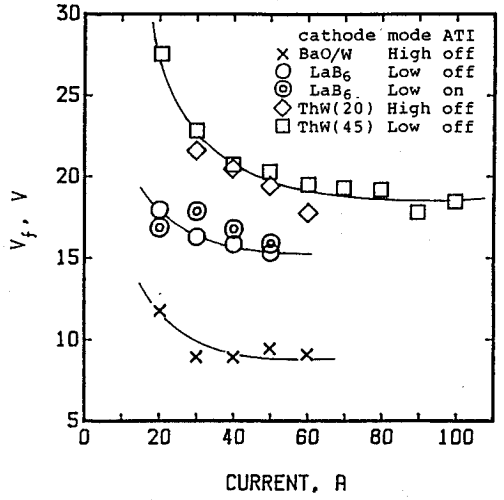

Fig. 14 V_f vs current characteristics for various cathode materials.

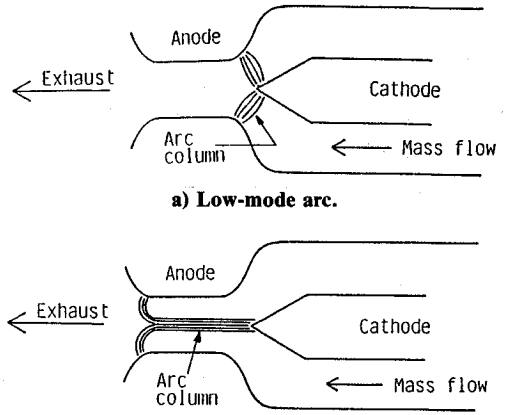

a) Low-mode arc.

b) High-mode arc.

Fig. 15 Schematic view of arc column.

tional cooling is rather trivial. Therefore, the active cooling of the cathode is concluded to be unnecessary.

The ATI propellant supply enhances the discharge voltage and decreases the thermal efficiency, as shown in Figs. 6 and 8, respectively. This results from the following reasons: 1) an increase of mass flow rate requires extra power for heating and ionization; 2) ATI modifies the arc discharge in equilibrium to a new condition of higher voltage; generally, near an anode, the thermal equilibrium is established by the balance of the electron acceleration by the fall voltage with the anode heat loss; 3) in the case of the low mode, the gas injected transpirationally from the surface of the constrictor is not directly heated by the arc discharge and is exhausted from the nozzle; consequently, a great decrease of the thermal efficiency results. The usefulness of ATI is dependent on whether the injected mass in the upstream region of the arc attachment is smoothly heated in the arc attachment without disturbing it. From the operational viewpoint, the feasibility of ATI seems to rely upon the porous electrode material. The pure tungsten is known to be susceptible to thermal stress, i.e., likely to be cracked. The porous tungsten is duly more susceptible and a better material is needed before making any conclusions about performance of ATI.

Summary

The following are the new findings from the present experiment. A thermal efficiency of 64.9% was obtained at about 1 kW input power with the BaO/W cathode. When the arc positive column was constricted at the anode throat, high thermal efficiency was obtained. In the case of a low-power arcjet, the cathode material should be provided with such characteristics as low work function and high thermal shock resistance, which contribute to high thermal efficiency and long-term durability, respectively. The total electron flux that the cathode can supply seems to control the discharge mode, i.e., either the high or low mode, for the given anode condition. Transpirational cooling at both the cathode and anode was found to be inefficient for a low-power arcjet.

References

[1]Wallner, L. E. and Czika, J. Jr., "Arc-jet Thruster for Space Propulsion," NASA TN D-2868, 1964.

[2]John, R. R., Connors, J. F., and Bennet, S., "Thirty Day Endurance Test of a 30kW Arc Jet Engine," AIAA Paper 63-274, June 1963.

[3]Todd, J. P. and Sheets, R. E., "Development of a Regeneratively Cooled 30-kW Arcjet Engine," *AIAA Journal*, Vol. 3, Jan. 1965, pp. 122-126.

[4]Jack, J. R., "Theoretical Performance of Propellants Suitable," NASA TN D-682, 1960.

[5]Schoeck, P. A. and Eckert, E. R. G., "Experiments on the Transpiration Cooled Anode of an Electric Arc," *Proceedings of 1961 Heat Transfer and Fluid Mechanics Institute,* Stanford University, Stanford, CA, 1961, pp. 193-207.

[6]Anderson, J. E. and Echert, E. R. G., "Transpiration Cooling of a Constricted Electric-Arc Heater," *AIAA Journal,* Vol. 5, April 1967.

[7]Winovich, W., "On the Equilibrium Sonic-Flow Method for Evaluating Electric-Arc Air-Heater Performance," NASA TN D-2132, 1963.

[8]Gerthsen, P. und Schutz, P., "Elektrodenfälle und Bogengradienten in der Quecksilber-Hochdruckentladung," *Zeitschrift für Physik,* Bd. 140, 1955.

[9]Nagamastu, H. T., "Experimental and Theoretical Study of a D.C. Arc in a Constant Diameter Nozzle Flow," IEEE Paper 81, SM 468-8, 1981.